

Effect of the Discretization and Neutronic Thermal Hydraulic Coupling on LWR Transients

Gerardo M. Grandi

Studsvik Scandpower, Inc.
504 Shoup Avenue, Suite 201
Idaho Falls ID 83402-3502
gerardo.grandi@studsvik.com

ABSTRACT

Coupled multiphysics problems solve different physical phenomena with time scales of varying orders of magnitude. These phenomena are coupled in a nonlinear way making it difficult to find an *accurate* and *efficient* solution. Many of the present generation of codes for LWR are based on 3-D neutronic nodal methods coupled with first order thermal hydraulic methods. Moreover, the spatial and temporal meshes used to solve each field are different reflecting the scales of each phenomenon.

This paper discusses the effect of the spatial and temporal discretization as well as the effect of different coupling schemes, with different level of implicitness, between the neutronic and core thermal hydraulics in SIMULATE-3K (S3K). S3K is a best estimate code used by many utilities, regulatory authorities and research institutes for the analysis of LWR transients that require the coupling of neutronic, fuel pin, and core hydraulic models. Examples of S3K applications are BWR stability analysis, fast anticipated operational occurrences, with or without scram, and reactivity initiated transients. Three different applications will be discussed in this paper to illustrate the effect of the discretization and coupling methods in multiphysics problems, namely: the NEA PWR rod ejection, the Ringhals-1 BWR stability, and the Peach Bottom turbine trip benchmarks.

KEYWORDS

SIMULATE-3K, LWR transients, multiphysics , neutronic /hydraulic coupling

1. INTRODUCTION

SIMULATE-3K (S3K) was designed to be a best estimate tool employing a full two-group advanced nodal model and very detailed fuel pin and channel hydraulic models. The underlying premise of S3K is that by faithfully modeling the detailed assembly-by-assembly neutronic and thermal hydraulic behavior of the reactor core, S3K could be applied to many types of core transients. In particular, S3K is well suited for LWR transients in which there is a strong coupling between neutronic and thermal hydraulic: reactivity initiated transients [1], BWR stability analysis [2], and fast Anticipated Operational Occurrences (AOO) with or without scram [3-4].

An *accurate* and *efficient* solution of those transients is key when there are limitations in the resources (CPU time) available to perform the calculations. An example of this would be when S3K is used to predict the stability parameters in the BWR core surveillance system

GARDEL [5], or as part of software to evaluate possible core loadings during core design.

The nonlinear coupling between the neutronic and channel thermal hydraulic models makes it quite a challenge to find an *accurate* and *efficient* solution for LWR transients. For example, the spatial and temporal discretization affects the stability parameter (decay ratio and natural frequency) calculations; key parameters of reactivity insertion accidents (peak powers, fuel temperatures, and fuel enthalpies) are sensitive to the degree of implicitness in the coupling between the neutronic and thermal hydraulic models. Therefore, understanding the effect of the discretization on the solution is more than an academic exercise.

2. MODELS

In what follows, brief descriptions of the neutronic, fuel pin, and channel hydraulic models of S3K are provided. Special emphasis is paid to the numerical methods used to integrate the governing equations, and the coupling between the different models.

2.1. Neutronic Model

The S3K neutronic model solves the transient three-dimensional, two-group neutron diffusion equations, including a six group model for delayed neutron precursors. S3K dynamically tracks the nodal concentrations of fission products and accounts for the neutron sources due to spontaneous fissions, alpha-n interactions from actinide decay, and gamma-n interactions from long-term fission product decay. Decay heat sources are modeled by using the ANSI/ANS 5.1 standard.

The basic spatial integration model is formed via transverse integration of the 3-D neutron diffusion equations separately over each spatial direction. This procedure creates an equivalent set of three one-dimensional equations coupled via a transverse leakage term. The flux distribution is expanded in terms of fourth-order polynomials in each direction [6],

$$\Phi_g(u) = \bar{\Phi}_g + \sum_{i=1}^4 \varphi_{g,i} \cdot u^i \quad (1)$$

and thus the spatial gradient of the flux can be analytically represented by third-order polynomials. This procedure yields the spatial coupling equations for the two-group neutron fluxes.

The frequency transform method is used for the time integration of the transient diffusion equations. This method separates the flux (Φ) into two components, one with a pure exponential time dependence, and the other (Ψ) with primarily spatial (and weak temporal) dependence. Thus, for each node it is assumed that,

$$\Phi_g^{n+1}(r, t) = e^{\Omega^{n+1}(t^{n+1}-t^n)} \Psi_g^{n+1}(r, t) \quad (2)$$

Each time step a new value for the nodal transformation frequency (Ω^{n+1}) is calculated from the core average thermal neutron flux as,

$$\Omega^{n+1} = \frac{1}{\Delta t} \ln \left(\frac{\Phi_2^{n+1}}{\Phi_2^n} \right) \quad (3)$$

Note that the nodal transformation frequency is based on the thermal flux. This assumption is justified because the time step used to integrate the diffusion equations ($10^{-1} - 10^{-3}$ sec.) is much greater than the moderation time ($\sim 10^{-5}$ sec). The time integration of the diffusion equations is performed using backward differences. The temporal terms in the neutron diffusion equations are discretized as,

$$\frac{\partial \Phi_g(r, t)}{\partial t} = \Omega^{n+1} \Phi_g^{n+1}(r) + e^{\Omega^{n+1}(t^{n+1}-t^n)} \frac{\Psi_g^{n+1}(r) - \Psi_g^n(r)}{\Delta t} \quad (4)$$

2.2 Fuel Pin Model

An average fuel pin per hydraulic node provides feedback between the neutronic and the channel hydraulic models: the average fuel temperature is used to evaluate cross sections, and the heat transferred to the coolant provides the hydraulic feedback. The heat conduction is governed by the one-dimensional, radial heat conduction equation, which in first order differences, fully implicit form can be written as,

$$\overline{C}_k (\overline{T}^{n+1} - \overline{T}^n) = \overline{L}_k (\overline{T}^{n+1}) + \overline{Q}_k^{n+1} \quad (5)$$

In Eq. (5), \overline{T} is the radial temperature distribution array $(T_1, T_2, \dots, T_N)^T$, \overline{C}_k is a diagonal matrix representing the volumetric heat capacity (ρC_p) , \overline{L}_k is a tri-diagonal matrix representing the discrete heat conduction operator and \overline{Q}_k^{n+1} is the vector that represents the heat sources. Note that pin temperatures are computed using a fully implicit scheme. All the material properties in \overline{C}_k and \overline{L}_k are temperature- and burnup- dependent.

Boundary conditions for Eq. (5) are the imposition of symmetry at the fuel pin centerline and the specification of the clad outer wall heat flux. The convective heat transfer coefficient between the clad and the bulk fluid is determined from one of several different possible modes of heat transfer according to a classical boiling formulation. It is important to mention that heat transfer coefficients are solved at each time step by nonlinear iteration between the fuel pin and hydraulic channel models.

2.3 Hydraulic Channel Model

The core is represented with one thermal hydraulic channel per fuel assembly with no cross flow. The channel hydraulic is a five-equation model: vapor and liquid mass conservation, vapor and liquid energy conservation and mixture momentum conservation. The hydraulic primitive variable set solved for, comprises the phasic mass fluxes G_v and G_l , phasic enthalpies h_v and h_l , pressure P , and void fraction α . In addition to the conservation equations, closure relationships exist for each phasic density (ρ_l and ρ_v), defined as a function of the pressure and phasic enthalpy. Water properties are evaluated at the core exit pressure. The general drift formulation for the void fraction completes the set of equations to be solved. The concentration parameter and void-weighted drift velocity are calculated using the EPRI

correlation. The subcooled boiling model is taken from Lahey's mechanistic model.

All primitive variables, in the S3K channel hydraulics, are defined on a consistent edge-centered mesh. This is in contrast to many thermal hydraulic system codes which employ a staggered mesh, defining phasic velocities on the edge and phasic properties such as density and internal enthalpy at the cell center. The spatial discretization is obtained by performing volume integration from lower to upper mesh edge, thereby preserving node integral quantities appearing in the temporal derivative and source terms. The discretized governing equations have the following general form [7],

$$\frac{\bar{\chi}^{n+1} - \bar{\chi}^n}{\Delta t} + F(h_{v,j\pm\frac{1}{2}}^{n+1}, h_{l,j\pm\frac{1}{2}}^{n+1}, G_{v,j\pm\frac{1}{2}}^{n+1}, G_{l,j\pm\frac{1}{2}}^{n+1}, \alpha_{v,j\pm\frac{1}{2}}^{n+1}, P_{v,j\pm\frac{1}{2}}^{n+1}) = 0 \quad (6)$$

where $\bar{\chi}_j$ represents the conserved properties for the node j (phasic masses, phasic energies or mixture mass flux) and is itself a function of the leading and trailing edges primitive variables. The indices $n+1$ and n refer, respectively, to the current and previous time steps with regard to the primitive variables utilized in the evaluation of χ and F . For example, the final form for the spatial and time discretized liquid continuity equation in the node j of volume V_j , with flow areas $A_{j-\frac{1}{2}}$ and $A_{j+\frac{1}{2}}$ defined in the lower and upper mesh edges is,

$$\bar{\rho}_{l,j}^{n+1} - \bar{\rho}_{l,j}^n + \frac{\Delta t}{A_j \cdot \Delta z_j} (G_l A_{j+\frac{1}{2}}^{n+1} - G_l A_{j-\frac{1}{2}}^{n+1} + \bar{\delta}_j^n \Delta z_j) = 0 \quad (7)$$

where

$$\bar{\rho}_{l,j}^{n+1} = \frac{1}{2} \left((1-\alpha) \rho_l \Big|_{j+\frac{1}{2}}^{n+1} + (1-\alpha) \rho_l \Big|_{j-\frac{1}{2}}^{n+1} \right) \quad (8)$$

To study the truncation error, Eqs. (7) and (8) are simplified assuming: constant flow area ($A_{j+\frac{1}{2}} = A_{j-\frac{1}{2}} = A_j$), pure liquid ($\alpha = 0$), no phase change ($\delta = 0$), and constant liquid velocity (U). Under these approximations Eq. (7) reduces to,

$$\frac{1}{2} (\rho_l \Big|_{j+\frac{1}{2}}^{n+1} + \rho_l \Big|_{j-\frac{1}{2}}^{n+1}) - \frac{1}{2} (\rho_l \Big|_{j+\frac{1}{2}}^n + \rho_l \Big|_{j-\frac{1}{2}}^n) + \frac{U \cdot \Delta t}{\Delta z_j} (\rho_l \Big|_{j+\frac{1}{2}}^{n+1} - \rho_l \Big|_{j-\frac{1}{2}}^{n+1}) = 0 \quad (9)$$

Expanding Eq. (9) in Taylor series, and truncating to second order one obtains,

$$\frac{\partial \rho}{\partial t} + \frac{\partial \rho \cdot U}{\partial z} = \frac{U \cdot \Delta z_j}{2} \frac{\partial^2 \rho}{\partial z^2} - \frac{\Delta t}{2} \frac{\partial^2 \rho}{\partial t^2} + \left(\frac{\Delta z_j}{2} - U \cdot \Delta t \right) \frac{\partial^2 \rho}{\partial z \partial t} \quad (10)$$

Following Hirt [8], the second order time derivatives,

$$\begin{aligned}\frac{\partial^2 \rho}{\partial z \partial t} &= -U \frac{\partial^2 \rho}{\partial z^2} \\ \frac{\partial^2 \rho}{\partial t^2} &= -U^2 \frac{\partial^2 \rho}{\partial z^2}\end{aligned}\tag{11}$$

are replaced into Eq. (10),

$$\frac{\partial \rho}{\partial t} + \frac{\partial \rho U}{\partial z} = \frac{U^2 \Delta t}{2} \frac{\partial^2 \rho}{\partial z^2}\tag{12}$$

Eq. (12) shows that Eq. (6) is unconditionally stable with numerical diffusion ($\frac{U^2 \Delta t}{2}$) proportional to the time step size. In the present method, the numerical diffusion is minimized by reducing the time step towards zero. This is in contrast with explicit, upwind methods (e.g. TRACE) for which the time step size has to be chosen to match the Courant limit as closely as possible to minimize the numerical diffusion [9].

2.4 Coupling of the Neutronic and Hydraulic Channel Models

The hydraulic channel module is coupled to the neutronic via the fuel pin heat generation rate, which is directly determined from the neutronic power. In turn, the thermal hydraulics module provides the neutronic with the appropriate hydraulic data (moderator density and average fuel temperature) to permit cross section feedback with local thermal conditions. The coupling between the thermal hydraulics and the neutronic can be performed: (a) asynchronously (weak coupling), (b) synchronously (strong coupling), or (c) using a mixture of the asynchronous and synchronous coupling options (default coupling mode). By asynchronous coupling mode, it is implied that the results from one module calculation at the previous time step are used as input to the other module calculation for the current time step. In the synchronous coupling mode, the time step is repeated to fully-synchronize feedback variables between the thermal hydraulics and the neutronic. As mentioned before, the default coupling mode is a mix of the two options. Changes in key variables (e.g. power, moderator density, fuel temperature) are examined when a time step has been completed. If their fractional changes satisfy pre-defined criteria, the time step is accepted and the integration continues. If the fractional change in any of the monitored variables exceeds the criteria, a back step procedure is introduced. First, the time step size is reduced, taking into account the actual changes in the monitored variables during the rejected time step, and second the integration (of the rejected time step) is repeated with the smaller time step. The back step procedure may be repeated several times until the requested maximum fractional change is satisfied and the feedback variables are synchronized.

3. RESULTS

Over the years, S3K has been validated against many internationally recognized benchmarks. Three of these benchmarks will be analyzed in what follows to assess the influence of the discretization and the neutronic/hydraulic coupling, namely: the PWR rod ejection [10], the Ringhals-1 BWR stability [11], and the Peach Bottom turbine trip [12] benchmarks.

3.1 NEA PWR Rod Ejection Accident (REA) Benchmark

The problem consists in analyzing a rod ejection accident in a typical UO₂ PWR core at Hot Zero Power (HZP, 2775 W). A subset of the proposed scenarios is discussed in this paper, namely: A1) core octant with rotational symmetry, ejection of the central rod; B1) core octant with rotational symmetry, ejection of a peripheral rod, and C1) full core, ejection of a peripheral rod. The chosen spatial discretization for this problem is: radial mesh of 2x2 nodes per assembly ($\Delta x_{ASS} = 21.6$ cm) and 24 axial nodes ($\Delta z = 15.3$ cm).

As an example, Fig. 1 shows the power (red line) and centerline fuel temperature (blue line) evolution for case C1. Borkowski et al [13] showed that S3K is capable of calculating the peak power in very good agreement with the solution reported in reference [10]. The maximum deviation in power following a seven-decade increase is 19%. Reported deviations in the time of the peak power are in the order of 0.03 s. The agreement of the fuel centerline is excellent. Maximum centerline temperatures differ 5% at the most. These three parameters (power peak, time of maximum power, and peak centerline temperature) were chosen to evaluate the effect of the temporal discretization and of the neutronic/hydraulic coupling option. The reference solution was obtained using a small time step (0.1 ms), and the synchronized neutronic/hydraulic option. It was verified that the solution does not change with further time step refinement.

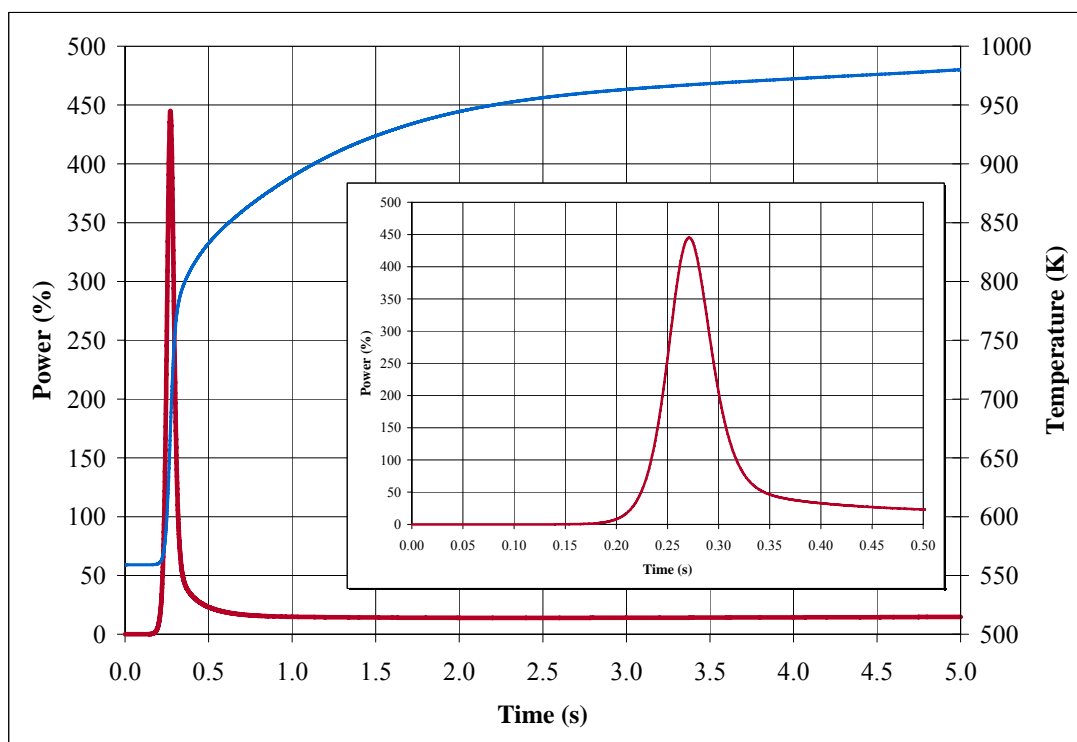


Fig. 1 PWR REA – Power and Centerline Fuel Temperature Evolution.

Table 1 shows the deviations using the synchronized coupling, and three different time steps: 100, 10, and 1 ms. Power peak and time of maximum power predictions are accurate only if the time step is lower than or equal to 10 ms. However, fuel centerline temperatures are accurately predicted even with a larger time step. Table 2 shows the same results, except that the asynchronous coupling has been selected. Significant differences in the power peak prediction are observed even with time steps as small as 10 ms.

The results with the default coupling option, and automatic time step are also shown in Table 2. Figure 2 shows power evolution (blue line) and the computed time step (red line) when the automatic time step algorithm is engaged for case C1. Note that the time step is reduced from the 100 ms (initial value) to 1 ms, during the first 0.1 s of the transient. This reduction occurs while the control rod is ejected. In this period of time, both the flux shape (ψ) and the amplitude are changing. Thus, small time steps are required to resolve the physics of the problem. Once the rod is completely ejected (0.1 s), the flux shape remains more or less constant. Consequently, the frequency transform method allows the simulation to be performed with larger time steps until the power level is high enough to start the thermal hydraulic feedback (approximately at 0.225 s). During the power excursion, the feedback affects not only the amplitude function but also the flux shape. Thus, the time step has to be reduced again. After the power peak, the flux shape has a weak temporal dependency and the frequency transform method allows the integration to continue with increasing time steps.

It is interesting to observe that the accuracy of the results produced by the default integration strategy (i.e. using an automatic time step selection and the back step procedure) is similar to the accuracy of the results computed with the synchronized coupling and a fixed time step of 1.0 ms. However, the computational cost (CPU time) is significantly reduced from 1400 s to 75 s.

Table 1. Deviations from reference solution with synchronous coupling

	Differences (%)			
	Ref. (%)	100 ms	10 ms	1 ms
Power peak				
Case A1	124.2	-31.2	-0.4	0.0
Case B1	238.4	-45.3	-6.3	-0.6
Case C1	453.4	-66.5	-17.7	-1.8
Time of power peak	Ref. (s)	100 ms	10 ms	1 ms
Case A1	0.55	-9.3	-9.3	-0.7
Case B1	0.53	14.3	1.0	0.0
Case C1	0.27	10.7	-0.4	0.0
Max. fuel temperature	Ref. (K)	100 ms	10 ms	1 ms
Case A1	959.5	0.6	0.2	0.0
Case B1	842.4	-0.3	0.0	0.0
Case C1	980.2	-2.3	-0.2	0.0

Table 2. Deviations from reference solution with asynchronous coupling

	Differences (%)					Default coupling & automatic time step
	Ref. (%)	100 ms	10 ms	1 ms		
Power peak						
Case A1	124.2	-68.5	-23.3	-0.1	1.4	
Case B1	238.4	225.4	0.0	-0.6	-3.5	
Case C1	453.4	132.7	3.7	-1.8	-1.5	
Time of power peak	Ref. (s)	100 ms	10 ms	1 ms		Default coupling & automatic time step
Case A1	0.55	1.9	0.2	0.0	-0.1	
Case B1	0.53	0.4	0.0	0.0	0.0	
Case C1	0.27	0.4	0.0	0.0	0.0	
Max. fuel temperature	Ref. (K)	100 ms	10 ms	1 ms		Default coupling & automatic time step
Case A1	959.5	-5.8	-0.4	0.0	0.2	
Case B1	842.4	7.6	0.0	0.0	0.0	
Case C1	980.2	67.1	0.2	0.0	0.0	

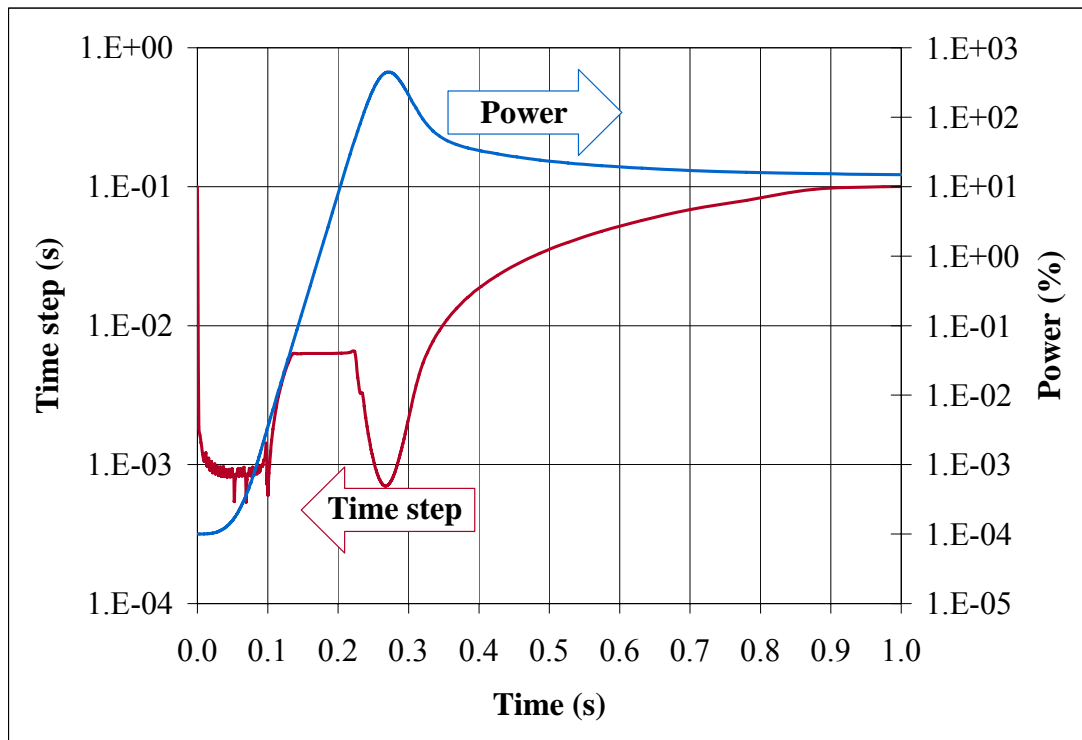


Fig. 2 PWR REA – Power Evolution and Time Step.

3.2 NEA Ringhals-1 Stability Benchmark

Ringhals-1 is a reactor of ASEA ATOM design with external recirculation pumps. Stability measurements were performed at BOC 14, 15, 16 and 17. These measurement campaigns were the basis for the NEA/OECD Stability Benchmark. S3K default stability calculations use 24-25 axial neutronic and hydraulic nodes in the core (i.e. a node size of approximately 15 cm.). Calculations are performed with a neutronic time step of 50 ms and 4 hydraulic time steps per neutronic time step (i.e. a hydraulic time step of 12.5 ms). Grandi et al. [2] showed that the default stability options produce accurate results. Decay ratios are computed with a bias of -0.03 and a standard deviation of 0.07. Natural frequencies are predicted with a bias of +0.02 and a standard deviation of 0.05.

Table 3 summarizes the results from a time step size sensitivity study performed for 3 cases of Ringhals-1 cycle 16. The values marked in bold are the ones obtained with the default time discretization. Figure 3 summarizes the results for a fixed neutronic time step (50 ms) and for a fixed hydraulic time step (12.5 ms) as "delta decay ratios", i.e. the difference between the calculated decay ratio for each selected time step and the decay ratio predicted by the default values. Note that an increase in the hydraulic time step, at constant neutronic time step (red line), has a clear damping effect as predicted by Eq. (12) above. If the neutronic time step is reduced, keeping the hydraulic time step constant (blue line), then the solution becomes less damped. The stabilizing effect is not due to numerical integration of the neutron diffusion equations, but to the coupling between the neutronic and the thermal hydraulic models. A smaller neutronic time step implies that the frequency of the thermal hydraulic feedback on cross sections increases.

Table 3. Ringhals-1 Benchmark. Effect of time step on decay ratio – Node size 15.3 cm

	Hydraulic time step (ms)	Neutronic time step (ms)		
		50.00	25.00	12.50
Case 9	50.00	0.77		
	25.00	0.86	0.82	
	12.50	0.92	0.87	0.86
	6.25	0.95	0.90	0.89
Case 4	50.00	0.53		
	25.00	0.59	0.56	
	12.50	0.63	0.60	0.59
	6.25	0.65	0.62	0.61
Case 1	50.00	0.42		
	25.00	0.47	0.44	
	12.50	0.50	0.47	0.46
	6.25	0.51	0.48	0.47

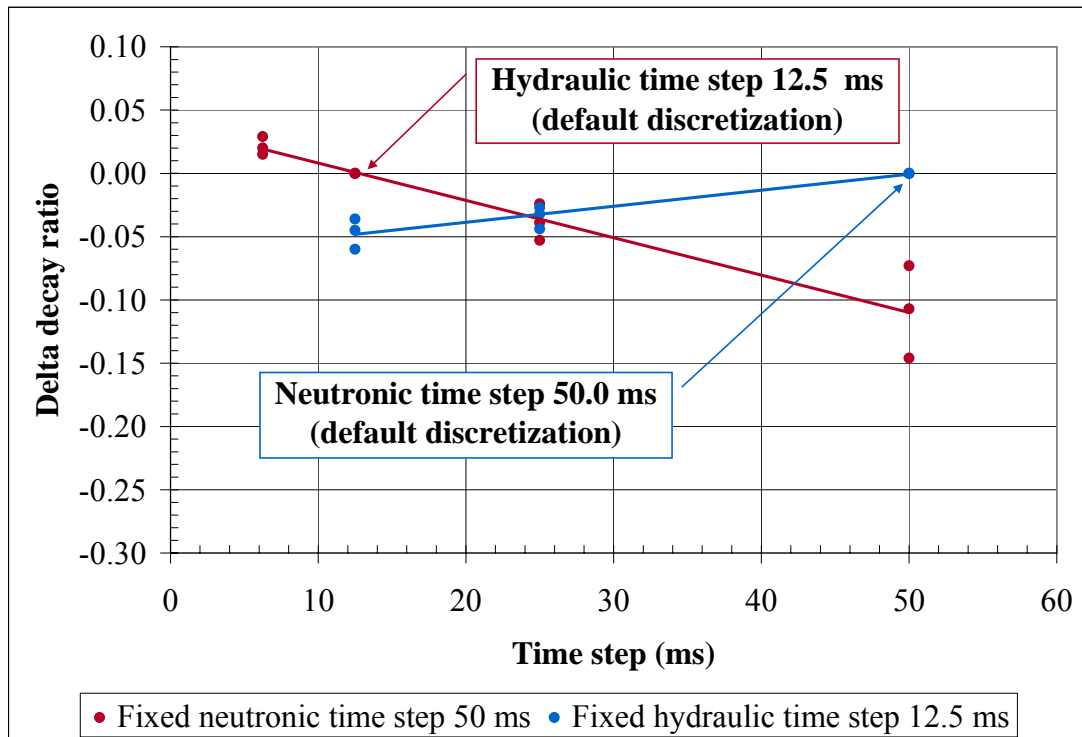


Fig. 3 Ringhals-1 Benchmark. Effect of the Time Step on Decay Ratio – Node Size 15.3 cm.

Table 4 summarizes the results from an axial nodalization sensitivity study performed for the above mentioned cases. The values marked in bold are the ones obtained with a typical axial discretization (node size 15.3 cm). A fixed time step of 12.5 ms was used to integrate both the neutronic and the thermal hydraulic equations. A very refined solution with 96 axial nodes (node size 3.8 cm), and a time step of 12.5 ms is also included.

Table 4. Ringhals-1 Benchmark. Effect of node size on decay ratio – Time step 12.5 ms

	Hydraulic node size(cm)	Neutronic node size (cm)			
		30.7	15.3	7.7	3.8
Case 9	30.7	0.58	0.78	0.76	
	15.3	0.72	0.86	0.85	
	7.7	0.75	0.91	0.87	
	3.8	0.76	0.92	0.89	0.89
Case 4	30.7	0.40	0.52	0.52	
	15.3	0.52	0.59	0.59	
	7.7	0.54	0.63	0.61	
	3.8	0.55	0.64	0.62	0.63
Case 1	30.7	0.35	0.39	0.38	
	15.3	0.41	0.46	0.46	
	7.7	0.43	0.49	0.48	
	3.8	0.44	0.50	0.48	0.49

Figure 4 summarizes the results as "delta decay ratios" for case 9. Results are sensitive to the neutronic and hydraulic axial mesh. The axial nodalization of the fuel assembly into 24 nodes (node size 15.3 cm) introduces a damping effect of less than 0.05 in decay ratio. The effect of the spatial discretization can be removed for all practical purposes by using 48 axial nodes (node size 7.7 cm).

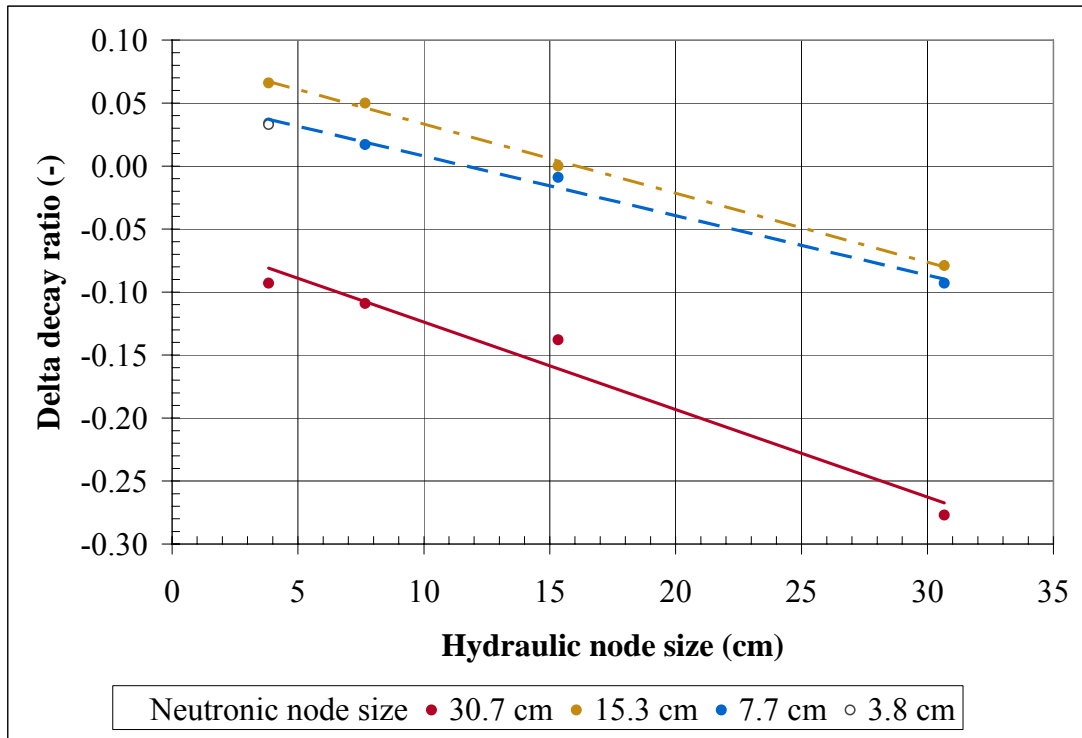


Fig. 4 Ringhals-1 Benchmark. Effect of the Hydraulic Node Size on Decay Ratio.

Table 4 and Fig. 5 clearly show that even if the neutronic model is third order in space, a refinement of the neutronic nodalization beyond 48 axial nodes (node size 7 cm) doesn't reduce or increase the numerical damping significantly.

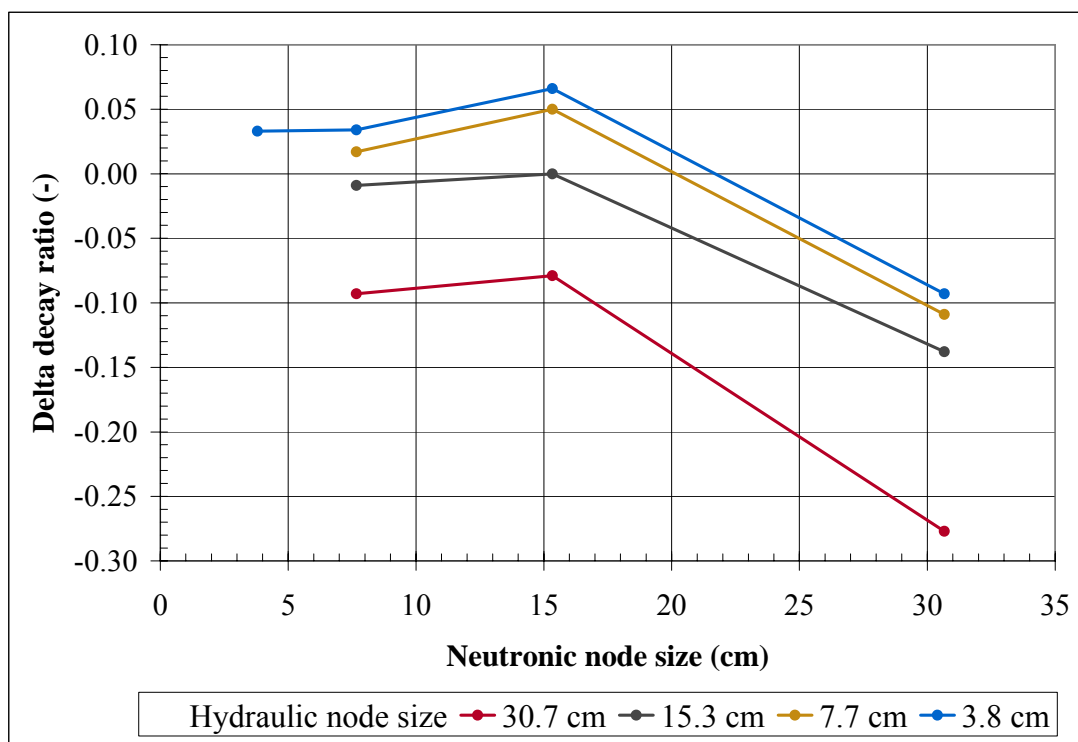


Fig. 5 Ringhals-1 Benchmark. Effect of the Neutronic Node Size on Decay Ratio.

3.3 NEA Peach Bottom Turbine Trip Benchmark

NEA/OECD proposed the Peach Bottom Turbine Trip Test 2 as a benchmark for a BWR plant transient. This pressurization transient, in which the coupling between the core and system dynamics plays an important role, includes plant data, making it very valuable for validating best-estimate analysis codes. The S3K model developed by Belblidia et al. [3] was capable of producing an accurate solution when compared to measurements. The peak relative power was well predicted at 4.43 (measured 4.52). The time of the peak is delayed by about 0.06 s from the start of turbine stop valve closure. The calculated steam dome pressure and core exit pressure follow the trend of the measurements: differences are lower than 50 kPa.

3.3.1 Effect of the spatial discretization

The Peach Bottom model was used to evaluate the effect of spatial discretization for fast operational transients. The effect of the fuel assemblies' axial nodalization, the radial mesh used to compute intra-pellet fuel temperatures, and the nodalization of the vessel model were studied. The reference solution was obtained with 24 axial neutronic (and hydraulic) nodes in the fuel assemblies, 10 volumes in the fuel pin, and 50 volumes per component in the BWR vessel model. The time step was set to the constant value of 10 ms.

The axial fuel assembly nodalization was decreased to 12 nodes per assembly, and increased to 48 nodes per assembly. Differences in peak power, maximum steam dome pressure, and core exit pressure are less than 1%. Differences in the minimum water level are less than 2%. The radial mesh in the fuel pin was decreased from 10 volumes to 5 volumes. Only the prediction of the peak power was significantly affected. The deviation in peak power is -3.5%. Differences in maximum steam dome pressure, core exit pressure, and minimum water level are less than 1%. If the fuel pin discretization is increased to 15 volumes, differences in peak

power are less than +0.8%. No significant differences are observed in the maximum steam dome pressure, and core exit pressure. For this particular transient, the nodalization of the vessel model plays no significant role.

3.3.2 Effect of the time discretization

The same model was used to evaluate the effect of time discretization for fast operational transients. The reference solution was obtained with 24 axial neutronic (and hydraulic) nodes in the fuel assemblies, 10 volumes in the fuel pin, and 50 volumes per component in the BWR vessel model. The time step was set to the constant value of 10 ms. Table 5 shows the deviations from the reference solution for 3 different constant time steps: 20, 50 and 100 ms. Significant differences, with respect to the reference solution, are only observed in peak power and water level. Table 5 also shows the differences when the automatic time step algorithm is engaged. Note that S3K automatic time step algorithm produces a solution that differs less than 1% with respect to the reference solution computed with fixed 10 ms time step. It is interesting to mention, that the computational cost is reduced by a factor of 5 compared to the solution computed with a 10 ms time step.

Table 5. Peach Bottom Turbine Trip. Effect of the time discretization – 24 axial nodes

Parameter	Ref. 10 ms	Differences (%)			
		20 ms	50 ms	100 ms	Automatic time step
Power peak (-)	4.255	-2.4	-2.8	4.0	0.8
Max. steam dome pressure (kPa)	7258.9	-0.1	-0.1	0.1	0.0
Max. core exit pressure (kPa)	7304.8	-0.1	-0.2	0.1	0.0
Min. water level (m)	1.29	0.8	1.6	1.6	0.8
CPU (s)	848	333	104	50	158

4. CONCLUSIONS

Results presented in this paper, and references [13], [2], and [3] show that S3K provides an accurate tool for analyzing a wide range of LWR transients. It was shown that time steps on the order of 10 ms are appropriate for BWR stability and BWR operational transients. Reactivity insertion accidents (PWR rod ejection and BWR rod drop) require time steps below 10 ms during control rod movements, and power excursions. Synchronization between the neutronic and thermal hydraulic fields is necessary if feedback effects are to be faithfully treated. The computational cost of the synchronization of the different fields is not significant, and requires, in most cases, only 2-5 back step iterations. The numerical diffusion of first order schemes neither limits the accuracy nor increases the uncertainty of results for LWR transients, provided that spatial and time discretizations capture the relevant physical phenomena. S3K numerical methods, with the spatial meshes described in this paper, are able to resolve each field in their natural scale. With its effective integration strategy (default neutronic/thermal hydraulic coupling and automatic time step), S3K is capable of producing *accurate* and *efficient* results for a large variety of LWR transients.

ACKNOWLEDGMENTS

This work benefited from discussions with Kord Smith of Studsvik Scandpower, Inc.

REFERENCES

1. G. Grandi, K. Smith, "S3K Explicit Fuel Pin Modeling during RIA's," *Trans. Am. Nucl. Soc.*, **96**, 627 (1985).
2. G. Grandi, L. Belblidia, and C. Jönsson, "BWR Stability Analyses With SIMULATE-3K - Benchmark Against Measured Plant Data," *Proceedings of Advances in Nuclear Fuel Management IV (ANFM IV)*, Hilton Head, South Carolina, USA, April 12-15 (2009).
3. L. Belblidia, G. Grandi, and C. Jönsson, "SIMULATE-3K Peach Bottom 2 Turbine Trip 2 Benchmark Calculations," *Nucl. Sci. Eng.*, **148**, 325 (2004).
4. C. Jönsson et al., "Cycle Specific BWR Reload Analysis Using SIMULATE-3K," *Proceedings of Advances in Nuclear Fuel Management IV (ANFM IV)*, Hilton Head, South Carolina, USA, April 12-15 (2009).
5. A. Noël, D. Dean, "GARDEL BWR On-line Monitoring Experience at Cooper and Monticello," *Trans. Am. Nucl. Soc.*, **97**, 737-738, November (2007).
6. K. Smith, "QPANDA: An Advanced Nodal Method for LWR Analysis," *Trans. Am. Nucl. Soc.*, **50**, 532 (1985).
7. D. Kropaczek, K. Smith and J. Borkowski, "A Fully-implicit, Five Equation Channel Hydraulics Model for SIMULATE-3K," *Proc. Joint Int. Conf. on Mathematical Methods and Supercomputing for Nuclear Applications*, Saratoga Springs, Florida, **1**, 1401 (1997).
8. C. Hirt, "Heuristic Stability Theory for Finite Difference Equations," *J. Comput. Phys.* **2**, 339 (1968).
9. Y. Xu et al., "Application of TRACE/PARCS to BWR Stability Analysis," *Proc. International Conference on the Physics of Reactors: Nuclear Power: A Sustainable Resource*, Interlaken, Switzerland (2008).
10. H. Finnemann, A. Galati, "NEACRP 3-D LWR Core Transient Benchmark: Final Specification," NEACRP-L335, Rev. 1, Nuclear Energy Agency Committee on Reactor Physics, January (1992).
11. T. Lefvert, "OECD/NEA Nuclear Science Committee BWR Stability Benchmark Final Specifications," NSC (94)15, Rev. 1, October (1994).
12. J. Solis et al., "Boiling Water Reactor Turbine Trip (TT) Benchmark: Final Specifications", **1**, NEA/NSC/DOC(2001)1, (2001).
13. J. Borkowski, J. Rhodes III, P. Esser and K. Smith, "Three Dimensional Transient Analysis Capability in SIMULATE-3," *Transactions of the American Nuclear Society*, **71**, 456 (1994).